Since January 2020 Elsevier has created a COVID-19 resource centre with free information in English and Mandarin on the novel coronavirus COVID-19. The COVID-19 resource centre is hosted on Elsevier Connect, the company's public news and information website.

Journal Pre-proof

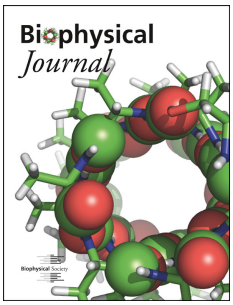

A potential interaction between the SARS-CoV-2 spike protein and nicotinic acetylcholine receptors

A. Sofia F. Oliveira, Amaurys Avila Ibarra, Isabel Bermudez, Lorenzo Casalino, Zied Gaieb, Deborah K. Shoemark, Timothy Gallagher, Richard B. Sessions, Rommie E. Amaro, Adrian J. Mulholland

PII: S0006-3495(21)00146-6

DOI: https://doi.org/10.1016/j.bpj.2021.01.037

Reference: BPJ 11000

To appear in: *Biophysical Journal*

Received Date: 11 November 2020

Accepted Date: 13 January 2021

Please cite this article as: Oliveira ASF, Ibarra AA, Bermudez I, Casalino L, Gaieb Z, Shoemark DK, Gallagher T, Sessions RB, Amaro RE, Mulholland AJ, A potential interaction between the SARS-CoV-2 spike protein and nicotinic acetylcholine receptors, *Biophysical Journal* (2021), doi: https://doi.org/10.1016/j.bpj.2021.01.037.

A potential interaction between the SARS-CoV-2 spike protein and nicotinic acetylcholine receptors

A. Sofia F. Oliveira,[a,b] Amaurys Avila Ibarra,[c] Isabel Bermudez,[d] Lorenzo Casalino,[e] Zied Gaieb,[e] Deborah K. Shoemark,[b,f] Timothy Gallagher,[a] Richard B. Sessions,[f] Rommie E. Amaro[e] and Adrian J. Mulholland[a*]

[a] Centre for Computational Chemistry, School of Chemistry, University of Bristol, Bristol BS8 1TS, UK

[b] Bristol Synthetic Biology Centre BrisSynBio, 24 Tyndall Ave, Bristol BS8 1TQ, UK

[c] Research Software Engineering, Advanced Computing Research Centre, University of Bristol, Bristol BS1 5QD, UK

[d] Department of Biological and Medical Sciences, Oxford Brookes University, Oxford OX30BP, UK

[e] Department of Chemistry and Biochemistry, University of California San Diego, La Jolla, CA, 92093 USA

[f] School of Biochemistry, University of Bristol, Bristol BS8 1DT, UK

*Corresponding author(s): adrian.mulholland@bristol.ac.uk

Abstract

Changeux *et al.* recently suggested that the SARS-CoV-2 spike protein may interact with nicotinic acetylcholine receptors (nAChRs), and that such interactions may be involved in pathology and infectivity. This hypothesis is based on the fact that the SARS-CoV-2 spike protein contains a sequence motif similar to known nAChR antagonists. Here, we use molecular simulations of validated atomically detailed structures of nAChRs, and of the spike, to investigate the possible binding of the Y674-R685 region of the spike to nAChRs. We examine the binding of the Y674-R685 loop to three nAChRs, namely the human α4β2 and α7 subtypes and the muscle-like αβγδ receptor from *Tetronarce californica*. Our results predict that Y674-R685 has affinity for nAChRs. The region of the spike responsible for binding contains a PRRA motif, a four-residue insertion not found in other SARS-like

coronaviruses. The conformational behaviour of the bound Y674-R685 is highly dependent on the receptor subtype: it adopts extended conformations in the α4β2 and α7 complexes, but is more compact when bound to the muscle-like receptor. In the α4β2 and αβγδ complexes, the interaction of Y674-R685 with the receptors forces the loop C region to adopt an open conformation, similar to other known nAChR antagonists. In contrast, in the α7 complex, Y674-R685 penetrates deeply into the binding pocket where it forms interactions with the residues lining the aromatic box, namely with TrpB, TyrC1 and TyrC2. Estimates of binding energy suggest that Y674-R685 forms stable complexes with all three nAChR subtypes. Analyses of simulations of the glycosylated spike show that the Y674-R685 region is accessible for binding. We suggest a potential binding orientation of the spike protein with nAChRs, in which they are in a non-parallel arrangement to one another.

Statement of significance

It was recently suggested that the SARS-CoV-2 spike protein may interact with nicotinic acetylcholine receptors, and that such interactions may be involved in pathology and infectivity. We investigate this hypothesis by molecular dynamics simulations. Our results predict that a viral spike-protein peptide (adjacent to the furin cleavage site) exhibits favourable binding affinity to nicotinic acetylcholine receptors and suggest subtype-specific dynamics for the peptide. We show that this peptide is accessible in the fully glycosylated spike. We model how the spike may interact with these receptors, and find that interaction is possible with the two proteins in a non-parallel arrangement.

Introduction

The severe acute respiratory syndrome coronavirus-2 (SARS-CoV-2) is a novel strain of coronavirus that first appeared in China in late 2019 and causes the potentially fatal disease COVID-19. This virus initially infects respiratory epithelial cells by binding to the angiotensin-converting 2 enzyme (ACE2) receptor (1). Although predominantly recognized as a respiratory disease (2, 3), SARS-CoV-2 also causes severe inflammation and damage in other organs (4-7). Under certain conditions (and as with other coronaviruses (8)), SARS-CoV-2 may enter the central nervous system (CNS) through the bloodstream by disrupting the blood-brain barrier or infecting the peripheral nerves (e.g. (7, 9-12)).

Since it emerged as a human pathogen, SARS-CoV-2 has caused more than 80.8 million confirmed cases of COVID-19 and more than 1.7 million deaths worldwide, as of 28th December, 2020 (13). Several major risk factors for the development of COVID-19 have been identified, including age,

heart disease, diabetes and hypertension (14). Given the apparently low prevalence of smokers among hospitalised COVID-19 patients (15-17), it was proposed that nicotine may offer some protective value to mitigate COVID-19 (the 'protection' hypothesis)(15). It has been suggested that medicinal nicotine (either in patches, gum, or electronic delivery systems) should be investigated as a therapeutic option for this disease (e.g. (15, 18)). Clinical trials for nicotine are underway (e.g. https://clinicaltrials.gov/ct2/show/NCT04429815). Alternative explanations to the protection hypothesis have been proposed (19): the first relates to the failure in correctly identifying smokers upon hospital admission (19), and the second is that hospitalised COVID-19 patients may be less likely to smoke as their comorbidities motivate them to quit ('smoking cessation' hypothesis)(19).

Based on the early observations of the lower than expected smoking prevalence in hospitalised COVID-19 patients, Changeux and colleagues suggested a role for nicotinic acetylcholine receptors (nAChRs) in the pathophysiology of COVID-19 via a direct interaction between these receptors and the viral spike glycoprotein (20). This suggestion was based in the fact that the spike protein contains a sequence motif similar to known nAChR antagonists (20) (**Figure S1**), such as α-bungarotoxin from *Bungarus multicinctus* and glycoprotein from *Rabies lyssavirus* (formerly *Rabies virus*). Changeux *et al*. and others also proposed that COVID-19 might be controlled or mitigated by the use of nicotine, if the latter can compete with the virus for binding to these receptors (e.g. (9, 18, 20-24)). If interactions with nAChRs are important, they may be relevant for some of the systemic effects observed in COVID-19.

nAChRs are cation channels that belong to the pentameric ligand-gated ion channel family (25). They are present in both the peripheral (at the skeletal neuromuscular junction and in the autonomic nervous system) and CNS (26). The neuronal receptors have emerged as important targets for the treatment of Alzheimer's disease, schizophrenia, pain and nicotine addiction (26, 27). Mutations of muscle nAChR can cause congenital myasthenia gravis (27). A large repertoire of nAChR subtypes differ in the homo- or heteromeric assembly of five monomers arranged around a central channel axis (28-30). Each nAChR subtype shows different selectivity for agonists and antagonists (28-30). All nAChRs share the same basic architecture (**Figure 1B**), formed of a large N-terminal extracellular domain (ECD), where the agonist binding site is located; a transmembrane domain (TMD) surrounding the ion channel; an intracellular domain (ICD); and a short extracellular C-terminal domain (CTD) (28-30) The ligand-binding pocket is located at the interface between two neighbouring subunits (**Figure 1B**) and is formed by loops A, B and C from the principal subunit and D, E and F from the complementary subunit (**Figure S2**). The α4β2 nAChR is the most prevalent heteromeric subtype in the brain: it is implicated in diverse processes such as cognition, mood and reward, and is necessary for nicotine addiction (28-31). The homomeric α7 nAChR is also abundant and widely expressed in the CNS, where it contributes to cognition, sensory processing and attention (32). The α7 subtype is also expressed on a variety of non-neuronal cells, such as immune cells,

astrocytes, microglia, endothelial cells, where it contributes to anti-inflammatory pathways (33-35). Due to its role in the downregulation of the production of pro-inflammatory cytokines (33-35), it has been suggested that the α7 nAChR may be involved in the hyper-inflammation response that can be caused by SARS-CoV-2 (9, 18, 24, 36). The muscle-type receptor derived from the electric organ of *Tetronarce californica* (formerly *Torpedo californica*) is one the most extensively studied nAChRs, and has provided significant structural insight into this receptor family. It is formed by two α and one each of β, δ and γ subunits, and has high sequence similarity (55%-80% identity) with its human counterpart (37). For this reason, and because its structure is available (38), we used it in this work as a proxy for the human muscle-type nAChRs. Muscle fatigue, myalgia and arthralgia are common symptoms in COVID-19 patients (e.g. (39-41)). However, it is still unclear if these symptoms result from direct muscle damage from viral infection or from the body's inflammatory response (7, 39).

According to Changeux *et al.*'s 'nicotinic hypothesis', direct interaction between SARS-CoV-2 and nAChRs occurs via a small region in the viral spike protein (20) (**Figures S3 and S4**). The spike is a fusion protein (42, 43) found on the surface of the virion that mediates entry into host cells. It is an extensively glycosylated homotrimer, with each monomer formed by three domains (**Figure 1A**): head, stalk and cytoplasmic tail (CT) (42). The head comprises two subunits: S1, which binds the ACE2 receptor on host cells (42), and S2, which facilitates membrane fusion (42). The spike contains two proteolytic cleavage sites (42): one ('furin cleavage' site) at the S1/S2 boundary thought to activate the protein (44) and a second in the S2 subunit that releases the fusion peptide (45). The region suggested by Changeux *et al*. to be directly involved in the interaction with nAChRs spans from Y674 to R685 and is located in the head region of the protein, at the interface between the S1 and S2 domains, immediately preceding the S1/S2 cleavage point (42) (**Figures 1A, S3 and S4**). Furin cleaves the peptide bond after R685, thus separating it from its neighbour S686 (e.g. before viral exit from the host cell) (44). Cleavage activation of viral glycoproteins is known to be important for infectivity and virulence (42, 44).

The Y674-R685 region contains a 4-residue, polybasic PRRA insertion not present in other SARS-CoV-related coronaviruses (46) that is homologous to several neurotoxins known to target nAChRs (20). In SARS-CoV-2, abrogation of the PRRA motif moderately affects virus entry into cells (42, 44). This motif has recently been shown experimentally to interact with neuropilin-1 receptors (47), T cell receptors (48), and host cell glycans, such as heparin sulfate (49, 50). The high sequence similarities between the Y674-R685 region and several known nAChR antagonists (**Figure S1**) suggests that this region of the SARS-CoV-2 spike protein may bind to nAChRs, potentially acting as an antagonist (20). Hence, it has been postulated that nicotine may have an effect in COVID-19 by competing and interfering with this binding. Note that an alternative region (G381 to K386 in the S1 subunit) in the spike protein has been hypothesized to interact with nAChRs (51), but glycosylation makes this unlikely.

Figure 1

Here, we use molecular simulations to examine the 'nicotinic hypothesis' proposed by Changeux *et al.* (20), in particular to test whether the SARS-CoV-2 spike protein can bind stably to nAChRs via the Y674-R685 region and identify interactions that may be involved in the stabilisation of the complexes. To test this, we have built structural models for the complexes formed by the 12-residue region from the spike (S-peptide) and the ECDs of three different nAChRs, namely the human α4β2, human α7 and muscle-like αβγδ receptor from *Tetronarce californica* (hereafter named αβγδ). These simulations build on our successful previous extensive simulations of nAChRs, which have e.g. identified a general mechanism for signal propagation in this receptor family (52-54), and simulations of the spike (55-58) and its interactions (47, 59).

Results and discussion

Interactions between the SARS-CoV-2 S-peptide and nAChRs

Structural models of the three SARS-CoV-2 S-peptide–nAChR complexes were built based on the cryoEM structure of the αβγδ receptor from *Tetronarce californica* with bungarotoxin (38). α-bungarotoxin is a neurotoxin that acts as a nAChR antagonist, directly competing with acetylcholine (60), and has high sequence similarity with the Y674-R685 region of the spike protein of SARS-CoV-2 (**Figure S1**). Twenty models were generated for each complex, and the one with the lowest Modeller objective function (61) (**Figures 2 and S7**) was used as the starting point for MD simulations (see the Supporting Information for more details). Three replicate simulations, each 300 ns long, were performed for each complex to investigate the peptide-receptor conformational behaviour and possible induced-fit effects.

Figure 2

At the beginning of the simulations, the S-peptide was located in the binding pocket, bound by interactions with both the principal and complementary subunits (**Figures 2 and S7**). A closeup view of the peptide-receptor interface reveals extensive contacts (**Figures 2B and S7B**), mainly with the

principal subunit. In all three complexes, the side-chain of R682 of the S-peptide binds as the recognised positively charged group, a strictly conserved pharmacophore of all nAChR ligands (62, 63). As can be seen in **Figure 2B**, the guanidinium group of R682 is well-positioned inside the aromatic box, forming several cation-π interactions with TyrC1 (α4Y223, α7Y210, αY214 in the human α4β2, human α7 and muscle-like αβγδ receptor from *Tetronarce californica*, respectively), TyrC2 (α4Y230, α7Y217, αY222) and TyrA (α4Y126, α7Y115, αY117). Note that these cation-π interactions do not entirely mimic the binding of nicotine, as no interactions with TrpB are present (64). R682 is part of the four-residue PRRA insertion not found in other SARS-like coronaviruses (46), and it forms part of the furin cleavage site located the boundary between the S1 and S2 subunits (42). Additional binding interactions with the peptide are also observed with different residues depending on the receptor subtype: in the α4β2 nAChR, hydrogen bonds involving the side-chains of α4Y223, α4E224, β2S192, β2D195 in the receptor and Q675, N679 and the main-chain nitrogen of A684 of the S-peptide are observed; in the α7 nAChR, two hydrogen bonds between α7D186 and α7Y210 in the receptor and S-peptide Q675 and Q677 are seen; in the αβγδ receptor from *Tetronarce californica*, hydrogen bonds involving αY214 and δD186 from the receptor and Q675, N679, R682 and R683 of the peptide are observed.

The simulations show distinct patterns of dynamical behaviour for the S-peptide in the different receptor subtypes. In the α4β2 and α7 complexes, the peptide showed high positional and conformational variability, while in the αβγδ complex, it generally remained in the same pose throughout the simulation (**Figures S8** and **S10**). Similar behaviour is observed for the peptides in the two binding pockets in each complex. When bound to the α4β2 and α7 nAChR, the peptide adopted many different binding modes inside the pocket, ranging from highly compact to fully extended conformations (**Figure S10**). In contrast, in the αβγδ receptor, the peptide was more compact (**Figure S10**). The range of the radius of gyration values for the S-peptide in all three complexes is similar to that observed in the simulations of the full-length glycosylated SARS-CoV-2 spike protein embedded in a viral membrane (55) (**Figure S6**). Principal component analysis (PCA) of the peptide dynamics revealed different conformational behaviour of the peptide in the three complexes. When bound to the muscle-like receptor, the peptide shows limited dynamical freedom: it explores a restricted conformational space spanned by the first two principal components (**Figure S11**).

The number of hydrogen bonds between the peptide and the receptors over the simulations was determined (**Figure S12**). Two more H-bonds are observed in the αβγδ complex than in the α4β2 and α7 receptors (**Figure S12**). These additional interactions with the complementary subunit (**Figure S12**) probably contribute to the increased stability of this complex and the more compact conformation of the peptide in the αβγδ receptor.

Analysis of the distribution of the distance between the R682 of the peptide and the conserved aromatic residues forming the aromatic box shows the distinctive behaviour of the peptide when bound to different receptors (**Figure S13**). Interactions with R682, TyrC1 and TyrC2 are quite frequent in all three complexes, being present more than 60% of the time. To examine how deeply into the binding pocket the peptide inserts, we monitored the interactions of R682 with TrpB, a residue lining the back wall of the nAChR aromatic box. TrpB (α4W182, α7W171 and αW173) is highly conserved across the nAChR family, and it makes cation-π and H-bond interactions with the positively charged group on the ligands (62, 63). In the α4β2 and αβγδ complexes, the S-peptide does not extend far into the pocket and interactions between R682 and TrpB are mostly absent (**Figure S13**). In contrast, in the α7 complex, the peptide binds more deeply into the hydrophobic cavity, adopting conformations that allow not only for the direct contact between R682 and TrpB (**Figures S14-S15**) but also achieve optimal core-binding interactions (**Figure 3**). In such configurations, other interactions are present in addition to those with TrpB, namely cation-π interactions with TyrC1 and TyrC2 (**Figure S15**). Although no direct contact between R682 and TyrA is observed, both residues are connected through a H-bond network mediated by Q675 from the S-peptide (**Figure S16**). This is significant because interactions with TyrA, TrpB, TyrC1 and TyrC2 are known to be critical for ligand binding and to modulate gating in the α7 subtype (65-67).

Figure 3

The binding of a ligand or a peptide can be expected to affect the conformational dynamics of the receptors (e.g. (52-54, 68-70)). To investigate this, the Root Mean Square Fluctuation (RMSF) profiles of the C_α atoms were determined for all three receptors. Distinct dynamic behaviours are observed for the binding site regions in the different subtypes (**Figures S17-S19**). These differences are mostly in loops C and F, two structural motifs important for binding and selectivity (66, 71, 72). Loop F shows decreased flexibility in the α4β2 complex, while loop C dynamics is more restricted in the muscle-like αβγδ receptor, compared to the other two subtypes.

At the beginning of the simulations, in all the three complexes, loop C adopted an open conformation due to the steric interference of the peptide. During the simulations, the αβγδ and α4β2 receptors mostly maintained this open conformation. In the α7 complex, as the peptide moved deeper into the binding pocket, loop C rotated inwards, adopting a semi-closed structure. Loop C capping is known to be important for the anchoring of the ligands in the binding pocket (66, 71) and has been suggested to be indirectly involved in gating (53, 73). A relationship between loop C position and ligand activation has also been proposed (72): agonists are proposed to stabilise more compact loop conformations while antagonists disfavour loop closing. On this basis, our findings suggest that the S-peptide may act as an antagonist in the αβγδ and α4β2 receptors, thus inhibiting gating. However, in the α7 subtype, it is unclear whether the peptide may be an agonist or antagonist, and whether it can promote

gating. How the S-peptide affects the different nAChRs may be relevant to understanding COVID-19 pathophysiology (9, 18, 24, 36).

Table 1: MM-PBSA relative binding energy values for the S-peptide in the human α4β2, human α7 and muscle-like αβγδ nAChR from *Tetronarce californica*. Numbers in brackets represent the standard deviations. Note that the values reported in this table are averaged over all replicates (see Table S1 for the ΔG_{bind} for the individual replicates) and do not contain the entropic contribution to the binding energy.

	Average ΔG_{bind} for the complexes (kJ/mol)		
	α4β2	**α7**	**αβγδ**
First pocket	–215.9 (80.4)	–184.5 (24.3)	–374.3 (98.5)
Second pocket	–215.7 (55.7)	–114.9 (46.6)	–391.5 (75.8)

A molecular mechanics Poisson–Boltzmann surface area (MM-PBSA) approach (74, 75) was used to calculate the free energy of binding of the S-peptide to the different receptors (**Tables 1** and **S1**). MM-PBSA calculations are an efficient and often useful method to estimate binding free energies (74, 75), and are widely used to study protein-ligand interactions in medicinal chemistry (76-78) including in drug design for nAChRs (79, 80). The favourable calculated binding energies suggest stable complex formation between the S-peptide and all three nAChRs (**Tables 1** and **S1**), with different binding affinities depending on the subtype.

Table 2: BUDE Alanine-scanning predicted average $\Delta\Delta G_{bind}$ for the hot-spots (–3 kJ/mol ≥ residue contribution ≤ 3 kJ/mol) in the first binding pocket of the receptors. The average value was calculated over the three replicates. Numbers in brackets represent the standard deviations (calculated over the 303 frames per complex). Note that the $\Delta\Delta G_{bind}$ corresponds to the difference between mutant and wild-type complexes, and as such positive $\Delta\Delta G_{bind}$ values mean that the mutation to alanine destabilizes the complex.

First binding pocket					
α4β2 receptor		**α7 receptor**		**Muscle-like αβγδ receptor**	
residue	$\Delta\Delta G_{bind}$ (kJ/mol)	residue	$\Delta\Delta G_{bind}$ (kJ/mol)	residue	$\Delta\Delta G_{bind}$ (kJ/mol)
β2D195	9.5 (3.6)	α7Y210	7.6 (2.2)	αY214	12.1 (2.6)
α4Y223	7.7 (2.0)	α7W77	5.1 (2.0)	δD201	6.1 (1.9)
α4Y230	3.7 (2.2)	α7Y115	3.8 (2.9)	δW197	4.6 (2.3)
β2W32	3.3 (1.7)	α7S188	3.7 (1.9)	δI199	4.0 (0.8)

	α7D186	3.1 (2.1)	δD186	3.9 (1.7)
			δE203	3.8 (2.0)
			αT215	3.1 (1.5)

In silico alanine-scanning mutagenesis was performed to identify important residues (referred to as 'hot-spots') in peptide−receptor association (**Figures S20-S22**). Hotspots are residues with high energetic contributions to the thermodynamic stability of a given complex (81). Alanine-scanning provides a detailed energy map of a protein-binding interface (81). Here, we used the fast *in silico* method, BudeAlaScan (81), in which every residue, for both receptor and peptide, is mutated (singly, in turn) to alanine. Hotspots are determined by the difference between the binding free energies of the alanine mutant and wild-type complexes ($\Delta\Delta G_{bind}$) (81). Hotspots were identified at the interface of the receptor, some of them common to all three subtypes (**Figure S23** and **Tables 2** and **S2**). In particular, TyrC1 (α4Y223, α7Y210, αY214) and the negatively charged residues in the upper part of loop F (β2D195, α7D186, δD201, δE203) strongly stabilise the complex. In the human α7 nAChR, the substitution of several key agonist-binding residues in the aromatic box (namely TyrA (α7Y115), TyrC1 (α7Y210), TrpB (α7W171) and TrpD (α7W77)) by alanine is also predicted to destabilise the interface between the peptide and the receptor. Of residues in the peptide, Y674, R682 and R685 are the major contributors to stabilizing the interface (**Figure S24**). This analysis reinforces the critical role of R682 in binding to nAChRs.

Accessibility of the SARS-CoV-2 S-peptide in MD simulations of the full-length glycosylated spike

Since the beginning of the pandemic, the computational structural biology/biomolecular simulation community has investigated the SARS-CoV-2 spike protein in different states and conditions, and the complexes that it forms (e.g. (55-59, 82-86)). Simulations have revealed the dynamics of the spike and its glycan shield (55, 57-59, 82, 83, 85, 86) and the effects of the binding of small molecules (56, 84). Here, to further explore the 'nicotinic hypothesis', we show that the Y674-R685 region (corresponding to the S-peptide) is accessible for binding, using the available MD simulations of the fully glycosylated full-length SARS-CoV-2 spike protein in the open and closed states by Casalino *et al.* (55) We note that in these models, the Y674-R685 region was modelled *de novo* as it was entirely (open spike) or partially (closed spike) missing in the initial cryoEM structures (42, 43) (for more details see Supporting Information). In these simulations, the Y674-R685 region adopts conformations potentially compatible with binding to nAChRs (**Figure 4A**). Our analysis reveals that the Y674-R685 loop is only weakly shielded by the glycans, and is predominantly solvent-exposed (**Figure 4** and **Figure S5**). Especially when the spike is in the closed state (**Figure 4B**), the Y674-

R685 loop appears highly accessible to a probe with a radius ranging from 1.4 Å to 15 Å. In contrast, in the open spike (**Figure 4C**), a larger variability of the accessible area is observed, preventing an unambiguous interpretation of the glycan shield effect on Y674-R685 for probes with a radius larger than 7 Å. The slightly different and less variable accessibility of the Y674-R585 loop observed in the closed spike when compared the open spike protein is in agreement with the sharper distribution of the radius of gyration calculated for this region in the closed spike (**Figure S6**). This behaviour might indicate different binding propensity of the S-peptide in the open and closed spike states. We hypothesize that it might be linked to a different packing of the three spike monomers in the two states. We note that the accessibility of this region makes it available to bind other receptors that may also bind the PRRA motif, such as neuropilin-1.

Figure 4

Conclusions

In summary, the findings reported here support the hypothesis that the SARS-CoV-2 spike protein can interact with nAChRs. Our calculations indicate stable binding of the spike protein to these receptors through a region adjacent to the furin cleavage site and corresponding to the Y674-R685 region. These calculations also show apparent subtype-specific interactions and dynamics for the Y674-R685 region. COVID-19 is known to cause a range of neurological (87, 88), muscular (39), and respiratory (89) symptoms and these predicted interactions may be relevant to understand the pathophysiology associated with this disease.

Our results predict that the Y674-R685 region of the spike protein has affinity for nAChRs. The region in the spike responsible for binding to nAChRs harbours the PRRA motif and shares high sequence similarity with neurotoxins known to be nAChR antagonists. The guanidinium group of R682 is the key anchoring point to the binding pocket, where it forms several interactions with the residues that form the aromatic box. Analysis of the structure and dynamics of the full-length glycosylated spike shows that the Y674-R685 region protrudes outside the glycan shield, is solvent accessible (**Figures 4** and **S5**) and is flexible (**Figure S6**), showing that it is accessible to bind to nAChRs (and to other receptors such as neuropilins (47)). Modelling the interaction between the full-length spike and nAChRs indicates that association is possible with the proteins in a non-parallel orientation to one another (**Figure S4**). Cryoelectron microscopy and tomography experiments, and coarse-grained simulations, show considerable bending and tilting of the spike. A tilt angle up to 60° relative to the normal axis of the membrane is observed (57, 58, 85, 90, 91). This flexibility of the spike protein would facilitate binding to host nAChRs.

Evidence that the interaction between the Y674-R685 region of the spike and nAChRs is possible comes from the recently characterized interaction of the spike protein with neuropilin-1 (47), which was shown to occur via the same region as the one proposed here. Having explored various possible orientations, we find that only approximately non-parallel arrangements of the spike and receptor allow for their interaction. This non-parallel interaction may not be immediately obvious, but it is consistent with other observations and is possible for two principal reasons: first, membrane curvature and deformation, and second, bending of the stalk of the spike. Experiments (e.g. cryoEM and tomography) and coarse-grained simulations show a significant degree of stalk bending is possible, and that the spike can adopt a wide range of conformations with different degrees of bending (57, 85, 90, 91) given by the three flexible hinges in the spike protein (85).

In the α4β2 and αβγδ complexes, the conformational dynamics of the bound Y674-R685 peptide are compatible with the hypothesis of it acting as an antagonist: it forces loop C to adopt an open conformation and prevents the formation of important interactions within the binding pocket. Intriguingly, in the α7 complexes, the peptide adopts binding modes that allow strong interactions within the aromatic box, raising the question of whether it promotes gating in this subtype. This is important because activation of α7 nAChR triggers anti-inflammatory signalling mechanisms in inflammatory cells, leading to a decrease in cytokine production, which may have relevance in understanding early COVID-19 pathology (9, 18, 24, 36). If nicotine does indeed prove to have any clinical value, it is likely that it would be due to interfering with the association with nAChRs. If so, nicotine analogues (e.g. smoking cessation agents such as varenicline (92), cytisine (93) and potentially cytisine variants (54)) could also find useful application for COVID-19.

Given the promising results presented here, structural, mutational and single-channel studies will be of interest to test the importance of the interactions of the SARS-CoV-2 spike with nAChRs, and the potential relevance of these interactions to pathology and infectivity in COVID-19. To assist with further investigations, we make our simulation files and datasets available and openly accessible, in accordance with the sharing principles agreed to by our community for simulations relevant to COVID-19 (94).

Supporting citations

References (20, 27, 38, 42, 43, 47, 52-55, 60, 61, 63, 64, 74, 75, 81, 95-123) appear in the Supporting Material.

Acknowledgements

AJM and ASFO thank EPSRC (grant number EP/M022609/1) and the Elizabeth Blackwell Institute for Health Research, University of Bristol, for financial support (Elizabeth Blackwell Institute Rapid Response Funding Call (COVID-19)). MD simulations were carried out using the computational facilities of the Advanced Computing Research Centre, University of Bristol (http://www.bris.ac.uk/acrc) and using Oracle Public Cloud Infrastructure (https://cloud.oracle.com/en_US/iaas) under an award for COVID-19 research. We thank Dr Simon Bennie and Dr Jonathan Barnoud for help with the Cluster-in-the-cloud and the creation of a scalable cluster on the Oracle Cloud. AJM, ASFO, RBS and DKS also thank EPSRC for provision of ARCHER HPC time through HECBioSim (HECBioSim.ac.uk) under a COVID-19 award. REA acknowledges support from NIH (GM132826), NSF RAPID (MCB-2032054), an award from the RCSA Research Corp. and a UC San Diego Moore's Cancer Center 2020 SARS-COV-2 seed grant. REA, LC and ZG thank the Texas Advanced Computing Center (TACC) Frontera team and acknowledge computer time made available through a Director's Discretionary Allocation (made possible by the NSF award OAC-1818253).

Author contributions

Conceptualization/design of the work: ASFO and AJM; Acquisition and analysis of the data: ASFO, AAI, LC and ZG; Writing of the manuscript: ASFO, AAI, LC and AJM; Review & Editing of the manuscript: ASFO, AJM, IB, ZG, TG, DKS, RBS and REA; Funding Acquisition: TM, REA and AJM.

Competing interests

The authors declare no competing interests.

References

1. Yan, R., Y. Zhang, Y. Li, L. Xia, Y. Guo, and Q. Zhou. 2020. Structural basis for the recognition of SARS-CoV-2 by full-length human ACE2. *Science* 367:1444-1448.
2. Rothan, H. A., and S. N. Byrareddy. 2020. The epidemiology and pathogenesis of coronavirus disease (COVID-19) outbreak. *J Autoimmun* 109:102433.
3. Lake, M. A. 2020. What we know so far: COVID-19 current clinical knowledge and research. *Clin Med (Lond)* 20:124-127.
4. Puntmann, V. O., M. L. Carerj, I. Wieters, M. Fahim, C. Arendt, J. Hoffmann, A. Shchendrygina, F. Escher, M. Vasa-Nicotera, A. M. Zeiher, M. Vehreschild, and E. Nagel.

2020. Outcomes of cardiovascular magnetic resonance imaging in patients recently recovered from coronavirus disease 2019 (COVID-19). *JAMA Cardiol* 5:1265-1273.

5. Varga, Z., A. J. Flammer, P. Steiger, M. Haberecker, R. Andermatt, A. S. Zinkernagel, M. R. Mehra, R. A. Schuepbach, F. Ruschitzka, and H. Moch. 2020. Endothelial cell infection and endotheliitis in COVID-19. *Lancet* 395:1417-1418.
6. Puelles, V. G., M. Lütgehetmann, M. T. Lindenmeyer, J. P. Sperhake, M. N. Wong, L. Allweiss, S. Chilla, A. Heinemann, N. Wanner, S. Liu, F. Braun, S. Lu, S. Pfefferle, A. S. Schröder, C. Edler, O. Gross, M. Glatzel, D. Wichmann, T. Wiech, S. Kluge, K. Pueschel, M. Aepfelbacher, and T. B. Huber. 2020. Multiorgan and renal tropism of SARS-CoV-2. *N Engl J Med* 383:590-592.
7. Zhang, Y., X. Geng, Y. Tan, Q. Li, C. Xu, J. Xu, L. Hao, Z. Zeng, X. Luo, F. Liu, and H. Wang. 2020. New understanding of the damage of SARS-CoV-2 infection outside the respiratory system. *Biomed Pharmacother* 127:110195.
8. Desforges, M., A. Le Coupanec, P. Dubeau, A. Bourgouin, L. Lajoie, M. Dubé, and P. J. Talbot. 2019. Human coronaviruses and other respiratory viruses: underestimated opportunistic pathogens of the central nervous system? *Viruses* 12:1-28.
9. Tizabi, Y., B. Getachew, R. L. Copeland, and M. Aschner. 2020. Nicotine and the nicotinic cholinergic system in COVID-19. *FEBS J* 287:3656-3663.
10. Baig, A. M., A. Khaleeq, U. Ali, and H. Syeda. 2020. Evidence of the COVID-19 virus targeting the CNS: tissue distribution, host-virus interaction, and proposed neurotropic mechanisms. *ACS Chem Neurosci* 11:995-998.
11. Baig, A. M., and E. C. Sanders. 2020. Heralding healthcare professionals: recognition of neurological deficits in COVID-19. *ACS Chem Neurosci* 11:1701-1703.
12. Alam, S. B., S. Willows, M. Kulka, and J. K. Sandhu. 2020. Severe acute respiratory syndrome coronavirus 2 may be an underappreciated pathogen of the central nervous system. *Eur J Neurol* 27:2348-2360.
13. Dong, E., H. Du, and L. Gardner. 2020. An interactive web-based dashboard to track COVID-19 in real time. *Lancet Infect Dis* 20:533-534.
14. Huang, C., Y. Wang, X. Li, L. Ren, J. Zhao, Y. Hu, L. Zhang, G. Fan, J. Xu, X. Gu, Z. Cheng, T. Yu, J. Xia, Y. Wei, W. Wu, X. Xie, W. Yin, H. Li, M. Liu, Y. Xiao, H. Gao, L. Guo, J. Xie, G. Wang, R. Jiang, Z. Gao, Q. Jin, J. Wang, and B. Cao. 2020. Clinical features of patients infected with 2019 novel coronavirus in Wuhan, China. *Lancet* 395:497-506.
15. Farsalinos, K., A. Barbouni, and R. Niaura. 2020. Systematic review of the prevalence of current smoking among hospitalized COVID-19 patients in China: could nicotine be a therapeutic option? *Intern Emerg Med* 15:845-852.
16. Guan, W. J., Z. Y. Ni, Y. Hu, W. H. Liang, C. Q. Ou, J. X. He, L. Liu, H. Shan, C. L. Lei, D. S. C. Hui, B. Du, L. J. Li, G. Zeng, K. Y. Yuen, R. C. Chen, C. L. Tang, T. Wang, P. Y. Chen, J. Xiang, S. Y. Li, J. L. Wang, Z. J. Liang, Y. X. Peng, L. Wei, Y. Liu, Y. H. Hu, P. Peng, J. M. Wang, J. Y. Liu, Z. Chen, G. Li, Z. J. Zheng, S. Q. Qiu, J. Luo, C. J. Ye, S. Y. Zhu, N. S. Zhong, and C. M. T. E. G. f. Covid-19. 2020. Clinical characteristics of coronavirus Disease 2019 in China. *N Engl J Med* 382:1708-1720.
17. Liu, W., Z. W. Tao, L. Wang, M. L. Yuan, K. Liu, L. Zhou, S. Wei, Y. Deng, J. Liu, H. G. Liu, M. Yang, and Y. Hu. 2020. Analysis of factors associated with disease outcomes in hospitalized patients with 2019 novel coronavirus disease. *Chin Med J (Engl)* 133:1032-1038.
18. Gonzalez-Rubio, J., C. Navarro-Lopez, E. Lopez-Najera, A. Lopez-Najera, L. Jimenez-Diaz, J. D. Navarro-Lopez, and A. Najera. 2020. Cytokine release syndrome (CRS) and nicotine in COVID-19 patients: trying to calm the storm. *Front Immunol* 11:1359.
19. Cohen, B., A. Nichols, S. Grant, Z. Blumenfeld, D. Dougherty, M. Alvarez, B. Ritz, and H. Lester. 2020. Successful cessation programs that reduce comorbidity may explain surprisingly low smoking rates among hospitalized COVID-19 patients. Qeios, doi:10.32388/WURFH0 (preprint posted May 27, 2020).
20. Changeux, J., Z. Amoura, F. Rey, and M. Miyara. 2020. A nicotinic hypothesis for Covid-19 with preventive and therapeutic implications. *CR Biol* 343:33-39.
21. Altable Pérez, M., and J. M. De la Serna. 2020. Neuroinvasion and viral reservoir in COVID-19. *Cureus* 12:e11014.

22. De Virgiliis, F., and S. Di Giovanni. 2020. Lung innervation in the eye of a cytokine storm: neuroimmune interactions and COVID-19. *Nat Rev Neurol* 16:645-652.
23. Leitzke, M., D. Stefanovic, J. J. Meyer, S. Schimpf, and P. Schönknecht. 2020. Autonomic balance determines the severity of COVID-19 courses. *Bioelectron Med* 6:22.
24. Dratcu, L., and X. Boland. 2020. Does nicotine prevent cytokine storms in COVID19? *Cureus* 12:e11220.
25. Wonnacott, S. 1997. Presynaptic nicotinic ACh receptors. *Trends in Neurosci* 20:92-98.
26. Gharpure, A., C. M. Noviello, and R. E. Hibbs. 2020. Progress in nicotinic receptor structural biology. *Neuropharmacology* 171:108086.
27. Cecchini, M., and J. P. Changeux. 2015. The nicotinic acetylcholine receptor and its prokaryotic homologues: structure, conformational transitions & allosteric modulation. *Neuropharmacology* 96:137-149.
28. Thompson, A. J., H. A. Lester, and S. C. Lummis. 2010. The structural basis of function in Cys-loop receptors. *Q Rev Biophys* 43:449-499.
29. Nemecz, A., M. S. Prevost, A. Menny, and P. J. Corringer. 2016. Emerging molecular mechanisms of signal transduction in pentameric ligand-gated ion channels. *Neuron* 90:452-470.
30. Changeux, J. P. 2018. The nicotinic acetylcholine receptor: a typical 'allosteric machine'. *Philos. Trans R Soc Lond B Biol Sci* 373:20170174.
31. Dineley, K. T., A. A. Pandya, and J. L. Yakel. 2015. Nicotinic ACh receptors as therapeutic targets in CNS disorders. *Trends Pharmacol Sci* 36:96-108.
32. Haydar, S., and J. Dunlop. 2010. Neuronal nicotinic acetylcholine receptors - targets for the development of drugs to treat cognitive impairment associated with schizophrenia and Alzheimer's disease. *Cur Top Med Chem* 10:144-152.
33. Martelli, D., D. G. Farmer, and S. T. Yao. 2016. The splanchnic anti-inflammatory pathway: could it be the efferent arm of the inflammatory reflex? *Exp Physiol* 101:1245-1252.
34. Tracey, K. J. 2002. The inflammatory reflex. *Nature* 420:853-859.
35. Maturo, M. G., M. Soligo, G. Gibson, L. Manni, and N. C. 2020. The greater inflammatory pathway-high clinical potential by innovative predictive, preventive, and personalized medical approach. *EPMA J* 11:1-16.
36. Manni, L., P. Tieri, and M. Soligo. 2020. A contribution to the hypothesis of nicotinic challenge as therapeutic option for COVID-19 patients. Qeios, doi: 10.32388/UJX3KN.2 (preprint posted April 27, 2020).
37. Unwin, N. 2013. Nicotinic acetylcholine receptor and the structural basis of neuromuscular transmission: insights from Torpedo postsynaptic membranes. *Q Rev Biophys* 46:283-322.
38. Rahman, M. M., J. Teng, B. T. Worrell, C. M. Noviello, M. Lee, A. Karlin, M. H. B. Stowell, and R. E. Hibbs. 2020. Structure of the native muscle-type nicotinic receptor and inhibition by snake venom toxins. *Neuron* 106:952-962.
39. Cipollaro, L., L. Giordano, J. Padulo, F. Oliva, and N. Maffulli. 2020. Musculoskeletal symptoms in SARS-CoV-2 (COVID-19) patients. *J Orthop Surg Res* 15:178.
40. Goyal, P., J. J. Choi, L. C. Pinheiro, E. J. Schenck, R. Chen, A. Jabri, M. J. Satlin, T. R. Campion, M. Nahid, J. B. Ringel, K. L. Hoffman, M. N. Alshak, H. A. Li, G. T. Wehmeyer, M. Rajan, E. Reshetnyak, N. Hupert, E. M. Horn, F. J. Martinez, R. M. Gulick, and M. M. Safford. 2020. Clinical characteristics of Covid-19 in New York city. *N Engl J Med* 382:2372-2374.
41. Vetter, P., D. L. Vu, A. G. L'Huillier, M. Schibler, L. Kaiser, and F. Jacquerioz. 2020. Clinical features of covid-19. *BMJ* 369:m1470.
42. Walls, A. C., Y. J. Park, M. A. Tortorici, A. Wall, A. T. McGuire, and D. Veesler. 2020. Structure, function, and antigenicity of the SARS-CoV-2 spike glycoprotein. *Cell* 181:281-292.
43. Wrapp, D., N. Wang, K. S. Corbett, J. A. Goldsmith, C. L. Hsieh, O. Abiona, B. S. Graham, and J. S. McLellan. 2020. Cryo-EM structure of the 2019-nCoV spike in the prefusion conformation. *Science* 367:1260-1263.
44. Davidson, A. D., M. K. Williamson, S. Lewis, D. Shoemark, M. W. Carroll, K. J. Heesom, M. Zambon, J. Ellis, P. A. Lewis, J. A. Hiscox, and D. A. Matthews. 2020. Characterisation

of the transcriptome and proteome of SARS-CoV-2 reveals a cell passage induced in-frame deletion of the furin-like cleavage site from the spike glycoprotein. *Genome Med* 12:68.

45. Apellániz, B., N. Huarte, E. Largo, and J. Nieva. 2014. The three lives of viral fusion peptides. Chemistry and Physics of Lipids. Elsevier Ireland Ltd, pp. 40-55.
46. Hoffmann, M., H. Kleine-Weber, and S. Pöhlmann. 2020. A multibasic cleavage site in the spike protein of SARS-CoV-2 is essential for infection of human lung cells. *Mol Cell* 78:779-784.
47. Daly, J. L., B. Simonetti, K. Klein, K. E. Chen, M. K. Williamson, C. Antón-Plágaro, D. K. Shoemark, L. Simón-Gracia, M. Bauer, R. Hollandi, U. F. Greber, P. Horvath, R. B. Sessions, A. Helenius, J. A. Hiscox, T. Teesalu, D. A. Matthews, A. D. Davidson, B. M. Collins, P. J. Cullen, and Y. Yamauchi. 2020. Neuropilin-1 is a host factor for SARS-CoV-2 infection. *Science* 370:861-865.
48. Cheng, M. H., S. Zhang, R. A. Porritt, M. Noval Rivas, L. Paschold, E. Willscher, M. Binder, M. Arditi, and I. Bahar. 2020. Superantigenic character of an insert unique to SARS-CoV-2 spike supported by skewed TCR repertoire in patients with hyperinflammation. *Proc Natl Acad Sci U S A* 117:25254-25262.
49. Zhang, Q., C. Z. Chen, M. Swaroop, M. Xu, L. Wang, J. Lee, A. Q. Wang, M. Pradhan, N. Hagen, L. Chen, M. Shen, Z. Luo, X. Xu, Y. Xu, W. Huang, W. Zheng, and Y. Ye. 2020. Heparan sulfate assists SARS-CoV-2 in cell entry and can be targeted by approved drugs in vitro. *Cell Discov* 6:80.
50. Clausen, T. M., D. R. Sandoval, C. B. Spliid, J. Pihl, H. R. Perrett, C. D. Painter, A. Narayanan, S. A. Majowicz, E. M. Kwong, R. N. McVicar, B. E. Thacker, C. A. Glass, Z. Yang, J. L. Torres, G. J. Golden, P. L. Bartels, R. N. Porell, A. F. Garretson, L. Laubach, J. Feldman, X. Yin, Y. Pu, B. M. Hauser, T. M. Caradonna, B. P. Kellman, C. Martino, P. L. S. M. Gordts, S. K. Chanda, A. G. Schmidt, K. Godula, S. L. Leibel, J. Jose, K. D. Corbett, A. B. Ward, A. F. Carlin, and J. D. Esko. 2020. SARS-CoV-2 infection depends on cellular heparan sulfate and ACE2. *Cell* 183:1043-1057.
51. Farsalinos, K., E. Eliopoulos, D. D. Leonidas, G. E. Papadopoulos, S. Tzartos, and K. Poulas. 2020. Nicotinic cholinergic system and COVID-19: in silico identification of an interaction between SARS-CoV-2 and nicotinic receptors with potential therapeutic targeting implications. *Int J Mol Sci* 21:5807.
52. Oliveira, A. S. F., D. K. Shoemark, H. R. Campello, T. Gallagher, R. B. Sessions, and A. J. Mulholland. 2019. Identification of the initial steps in signal transduction in the α4β2 nicotinic receptor: insights from equilibrium and nonequilibrium simulations. *Structure* 27:1171-1183.
53. Oliveira, A., C. Edsall, C. Woods, P. Bates, G. Nunez, S. Wonnacott, I. Bermudez, G. Ciccotti, T. Gallagher, R. Sessions, and A. Mulholland. 2019. A general mechanism for signal propagation in the nicotinic acetylcholine receptor family. *J Am Chem Soc* 141:19953-19958.
54. Campello, H. R., S. G. Del Villar, A. Honraedt, T. M. Viñas, A. S. F. Oliveira, K. E. Ranaghan, D. K. Shoemark, I. Bermudez, C. Gotti, R. B. Sessions, A. J. Mulholland, S. Wonnacott, and T. Gallagher. 2018. Unlocking nicotinic selectivity via direct C–H functionalisation of (–)-cytisine. *Chem* 4:1710-1725.
55. Casalino, L., Z. Gaieb, J. A. Goldsmith, C. K. Hjorth, A. C. Dommer, A. M. Harbison, C. A. Fogarty, E. P. Barros, B. C. Taylor, J. S. McLellan, E. Fadda, and R. E. Amaro. 2020. Beyond shielding: the roles of glycans in the SARS-CoV-2 spike protein. *ACS Cent Sci* 6:1722-1734.
56. Toelzer, C., K. Gupta, S. Yadav, U. Borucu, A. Davidson, M. Williamson, D. Shoemark, F. Garzoni, O. Staufer, R. Milligan, J. Capin, A. Mulholland, J. Spatz, D. Fitzgerald, I. Berger, and C. Schaffitzel. 2020. Free fatty acid binding pocket in the locked structure of SARS-CoV-2 spike protein. *Science* 370:725-730.
57. Casalino, L., A. Dommer, Z. Gaieb, E. P. Barros, T. Sztain, S. H. Ahn, A. Trifan, A. Brace, A. Bogetti, H. Ma, H. Lee, M. Turilli, S. Khalid, L. Chong, C. Simmerling, D. J. Hardy, J. D. C. Maia, J. C. Phillips, T. Kurth, A. Stern, L. Huang, J. McCalpin, M. Tatineni, T. Gibbs, J. E. Stone, S. Jha, A. Ramanathan, and R. E. Amaro. 2020. AI-driven multiscale simulations illuminate mechanisms of SARS-CoV-2 spike dynamics. bioRxiv, doi:10.1101/2020.11.19.390187 (preprint posted November 20, 2020).

58. Yu, A., A. J. Pak, P. He, V. Monje-Galvan, L. Casalino, Z. Gaieb, A. C. Dommer, R. E. Amaro, and G. A. Voth. 2020. A multiscale coarse-grained model of the SARS-CoV-2 virion. *Biophys J* In press.
59. Barros, E. P., L. Casalino, Z. Gaieb, A. C. Dommer, Y. Wang, L. Fallon, L. Raguette, K. Belfon, C. Simmerling, and R. E. Amaro. 2020. The flexibility of ACE2 in the context of SARS-CoV-2 infection. *Biophys J* In press.
60. Wang, G. K., and J. Schmidt. 1980. Primary structure and binding properties of iodinated derivatives of alpha-bungarotoxin. *J Biol Chem* 255:11156-11162.
61. Sali, A. 1995a. Comparative protein modeling by satisfaction of spatial restraints. *Mol Med Today* 1:270-277.
62. Dougherty, D. A. 2008. Cys-loop neuroreceptors: structure to the rescue? *Chem Rev* 108:1642-1653.
63. Corringer, P. J., F. Poitevin, M. S. Prevost, L. Sauguet, M. Delarue, and J. P. Changeux. 2012. Structure and pharmacology of pentameric receptor channels: from bacteria to brain. *Structure* 20:941-956.
64. Morales-Perez, C. L., C. M. Noviello, and R. E. Hibbs. 2016. X-ray structure of the human alpha 4 beta 2 nicotinic receptor. *Nature* 538:411-415.
65. Williams, D. K., C. Stokes, N. A. Horenstein, and R. L. Papke. 2009. Differential regulation of receptor activation and agonist selectivity by highly conserved tryptophans in the nicotinic acetylcholine receptor binding site. *J Pharmacol Exp Ther* 330:40-53.
66. Puskar, N. L., X. Xiu, H. A. Lester, and D. A. Dougherty. 2011. Two neuronal nicotinic acetylcholine receptors, alpha4beta4 and alpha7, show differential agonist binding modes. *J Biol Chem* 286:14618-14627.
67. Van Arnam, E. B., E. E. Blythe, H. A. Lester, and D. A. Dougherty. 2013. An unusual pattern of ligand-receptor interactions for the α7 nicotinic acetylcholine receptor, with implications for the binding of varenicline. *Mol Pharmacol* 84:201-207.
68. Suresh, A., and A. Hung. 2016. Molecular simulation study of the unbinding of alpha-conotoxin [Upsilon4E]GID at the alpha7 and alpha4beta2 neuronal nicotinic acetylcholine receptors. *J Mol Graph Model* 70:109-121.
69. Grazioso, G., J. Sgrignani, R. Capelli, C. Matera, C. Dallanoce, M. De Amici, and A. Cavalli. 2015. Allosteric modulation of alpha7 nicotinic receptors: mechanistic insight through metadynamics and essential dynamics. *J Chem Inf Model* 55:2528-2539.
70. Arias, H. R., D. Feuerbach, and M. Ortells. 2015. Functional and structural interaction of (-)-lobeline with human alpha4beta2 and alpha4beta4 nicotinic acetylcholine receptor subtypes. *Int J Biochem Cell Biol* 64:15-24.
71. Horenstein, N. A., T. J. McCormack, C. Stokes, K. Ren, and R. L. Papke. 2007. Reversal of agonist selectivity by mutations of conserved amino acids in the binding site of nicotinic acetylcholine receptors. *J Biol Chem* 282:5899-5909.
72. Nys, M., D. Kesters, and C. Ulens. 2013. Structural insights into Cys-loop receptor function and ligand recognition. *Biochem. Pharmacol.* 86:1042-1053.
73. Purohit, P., and A. Auerbach. 2013. Loop C and the mechanism of acetylcholine receptor-channel gating. *J Gen Physiol* 141:467-478.
74. Wang, C., D. Greene, L. Xiao, R. Qi, and R. Luo. 2017. Recent developments and applications of the MMPBSA method. *Front Mol Biosci* 4:87.
75. Genheden, S., and U. Ryde. 2015. The MM/PBSA and MM/GBSA methods to estimate ligand-binding affinities. *Expert Opin Drug Discov* 10:449-461.
76. Slynko, I., K. Schmidtkunz, T. Rumpf, S. Klaeger, S. Heinzlmeir, A. Najar, E. Metzger, B. Kuster, R. Schüle, M. Jung, and W. Sippl. 2016. Identification of highly potent protein kinase C-related kinase 1 inhibitors by virtual screening, binding free energy rescoring, and in vitro testing. *ChemMedChem* 11:2084-2094.
77. Evers, A., and T. Klabunde. 2005. Structure-based drug discovery using GPCR homology modeling: successful virtual screening for antagonists of the alpha1A adrenergic receptor. *J Med Chem* 48:1088-1097.
78. Raza, S., K. E. Ranaghan, M. W. van der Kamp, C. J. Woods, A. J. Mulholland, and S. S. Azam. 2019. Visualizing protein-ligand binding with chemical energy-wise decomposition

(CHEWD): application to ligand binding in the kallikrein-8 S1 Site. *J Comput Aided Mol Des* 33:461-475.

79. Grazioso, G., D. Y. Pomè, C. Matera, F. Frigerio, L. Pucci, C. Gotti, C. Dallanoce, and M. De Amici. 2009. Design of novel alpha7-subtype-preferring nicotinic acetylcholine receptor agonists: application of docking and MM-PBSA computational approaches, synthetic and pharmacological studies. *Bioorg Med Chem Lett* 19:6353-6357.
80. Grazioso, G., A. Cavalli, M. De Amici, M. Recanatini, and C. De Micheli. 2008. Alpha7 nicotinic acetylcholine receptor agonists: prediction of their binding affinity through a molecular mechanics Poisson-Boltzmann surface area approach. *J Comput Chem* 29:2593-2602.
81. Ibarra, A. A., G. J. Bartlett, Z. Hegedüs, S. Dutt, F. Hobor, K. A. Horner, K. Hetherington, K. Spence, A. Nelson, T. A. Edwards, D. N. Woolfson, R. B. Sessions, and A. J. Wilson. 2019. Predicting and experimentally validating hot-spot residues at protein-protein interfaces. *ACS Chem Biol* 14:2252-2263.
82. Sikora, M., S. Bulow, F. Florian E. C. Blanc, M. Michael Gecht, R. Roberto Covino, and G. Gerhard Hummer. 2020. Map of SARS-CoV-2 spike epitopes not shielded by glycans. bioRxiv, doi:10.1101/2020.07.03.186825 (preprint posted Jully 3, 2020).
83. Zimmerman, M., J. Porter, M. Ward, S. Singh, N. Vithani, A. Meller, U. Mallimadugula, C. Kuhn, J. Borowsky, R. Wiewiora, M. Hurley, A. Harbison, C. Fogarty, J. Coffland, E. Fadda, V. Voelz, J. Chodera, and G. Bowman. 2020. SARS-CoV-2 simulations go exascale to capture spike opening and reveal cryptic pockets across the proteome. bioRxiv, doi:10.1101/2020.06.27.175430 (preprint posted October 7, 2020).
84. Shoemark, D., C. Colenso, C. Toelzer, K. Gupta, R. Sessions, A. Davidson, I. Berger, C. Schaffitzel, J. Spencer, and A. Mulholland. 2020. Molecular simulations suggest vitamins, retinoids and steroids as ligands binding the free fatty acid pocket of SARS-CoV-2 spike protein. ChemRxiv, doi:10.26434/chemrxiv.13143761.v1 (preprint posted November 28, 2020).
85. Turoňová, B., M. Sikora, C. Schürmann, W. J. H. Hagen, S. Welsch, F. E. C. Blanc, S. von Bülow, M. Gecht, K. Bagola, C. Hörner, G. van Zandbergen, J. Landry, N. T. D. de Azevedo, S. Mosalaganti, A. Schwarz, R. Covino, M. D. Mühlebach, G. Hummer, J. Krijnse Locker, and M. Beck. 2020. In situ structural analysis of SARS-CoV-2 spike reveals flexibility mediated by three hinges. *Science* 370:203-208.
86. Fallon, L., K. Belfon, L. Raguette, Y. Wang, C. Corbo, D. Stepanenko, A. Cuomo , J. Guerra , S. Budhan , S. Varghese , R. Rizzo , and C. Simmerling. 2020. Free energy landscapes for RBD opening in SARS-CoV-2 spike glycoprotein simulations suggest key interactions and a potentially druggable allosteric pocket. ChemRxiv, doi:10.26434/chemrxiv.13502646.v1 (preprint posted December 31, 2020).
87. Ellul, M. A., L. Benjamin, B. Singh, S. Lant, B. D. Michael, A. Easton, R. Kneen, S. Defres, J. Sejvar, and T. Solomon. 2020. Neurological associations of COVID-19. *Lancet Neurol* 19:767-783.
88. Paterson, R. W., R. L. Brown, L. Benjamin, R. Nortley, S. Wiethoff, T. Bharucha, D. L. Jayaseelan, G. Kumar, R. E. Raftopoulos, L. Zambreanu, V. Vivekanandam, A. Khoo, R. Geraldes, K. Chinthapalli, E. Boyd, H. Tuzlali, G. Price, G. Christofi, J. Morrow, P. McNamara, B. McLoughlin, S. T. Lim, P. R. Mehta, V. Levee, S. Keddie, W. Yong, S. A. Trip, A. J. M. Foulkes, G. Hotton, T. D. Miller, A. D. Everitt, C. Carswell, N. W. S. Davies, M. Yoong, D. Attwell, J. Sreedharan, E. Silber, J. M. Schott, A. Chandratheva, R. J. Perry, R. Simister, A. Checkley, N. Longley, S. F. Farmer, F. Carletti, C. Houlihan, M. Thom, M. P. Lunn, J. Spillane, R. Howard, A. Vincent, D. J. Werring, C. Hoskote, H. R. Jäger, H. Manji, M. S. Zandi, and U. Q. S. N. H. f. N. a. N. C.-S. Group. 2020. The emerging spectrum of COVID-19 neurology: clinical, radiological and laboratory findings. *Brain* 143:3104-3120.
89. Yuki, K., M. Fujiogi, and S. Koutsogiannaki. 2020. COVID-19 pathophysiology: a review. *Clin Immunol* 215:108427.

90. Yao, H., Y. Song, Y. Chen, N. Wu, J. Xu, C. Sun, J. Zhang, T. Weng, Z. Zhang, Z. Wu, L. Cheng, D. Shi, X. Lu, J. Lei, M. Crispin, Y. Shi, L. Li, and S. Li. 2020. Molecular architecture of the SARS-CoV-2 virus. *Cell* 183:730-738.
91. Ke, Z., J. Oton, K. Qu, M. Cortese, V. Zila, L. McKeane, T. Nakane, J. Zivanov, C. J. Neufeldt, B. Cerikan, J. M. Lu, J. Peukes, X. Xiong, H. G. Kräusslich, S. H. W. Scheres, R. Bartenschlager, and J. A. G. Briggs. 2020. Structures and distributions of SARS-CoV-2 spike proteins on intact virions. *Nature* 588:498-502.
92. Hays, J. T., and J. O. Ebbert. 2008. Varenicline for tobacco dependence. *N Engl J Med* 359:2018-2024.
93. Etter, J. F. 2006. Cytisine for smoking cessation: a literature review and a meta-analysis. *Arch Intern Med* 166:1553-1559.
94. Amaro, R. E., and A. J. Mulholland. 2020. A community letter regarding sharing biomolecular simulation data for COVID-19. *J Chem Inf Model* 60:2653-2656.
95. Walsh, R. M., Jr., S. H. Roh, A. Gharpure, C. L. Morales-Perez, J. Teng, and R. E. Hibbs. 2018. Structural principles of distinct assemblies of the human alpha4beta2 nicotinic receptor. *Nature* 557:261-265.
96. Lester, H. A. 1972. Blockade of acetylcholine receptors by cobra toxin: electrophysiological studies. *Mol Pharmacol* 8:623-631.
97. Bateman, A., M. Martin, C. O'Donovan, M. Magrane, E. Alpi, R. Antunes, B. Bely, M. Bingley, C. Bonilla, R. Britto, B. Bursteinas, H. Bye-A-Jee, A. Cowley, A. Da Silva, M. De Giorgi, T. Dogan, F. Fazzini, L. Castro, L. Figueira, P. Garmiri, G. Georghiou, D. Gonzalez, E. Hatton-Ellis, W. Li, W. Liu, R. Lopez, J. Luo, Y. Lussi, A. MacDougall, A. Nightingale, B. Palka, K. Pichler, D. Poggioli, S. Pundir, L. Pureza, G. Qi, S. Rosanoff, R. Saidi, T. Sawford, A. Shypitsyna, E. Speretta, E. Turner, N. Tyagi, V. Volynkin, T. Wardell, K. Warner, X. Watkins, R. Zaru, H. Zellner, I. Xenarios, L. Bougueleret, A. Bridge, S. Poux, N. Redaschi, L. Aimo, G. Argoud-Puy, A. Auchincloss, K. Axelsen, P. Bansal, D. Baratin, M. Blatter, B. Boeckmann, J. Bolleman, E. Boutet, L. Breuza, C. Casal-Casas, E. de Castro, E. Coudert, B. Cuche, M. Doche, D. Dornevil, S. Duvaud, A. Estreicher, L. Famiglietti, M. Feuermann, E. Gasteiger, S. Gehant, V. Gerritsen, A. Gos, N. Gruaz-Gumowski, U. Hinz, C. Hulo, F. Jungo, G. Keller, V. Lara, P. Lemercier, D. Lieberherr, T. Lombardot, X. Martin, P. Masson, A. Morgat, T. Neto, N. Nouspikel, S. Paesano, I. Pedruzzi, S. Pilbout, M. Pozzato, M. Pruess, C. Rivoire, B. Roechert, M. Schneider, C. Sigrist, K. Sonesson, S. Staehli, A. Stutz, S. Sundaram, M. Tognolli, L. Verbregue, A. Veuthey, C. Wu, C. Arighi, L. Arminski, C. Chen, Y. Chen, J. Garavelli, H. Huang, K. Laiho, P. McGarvey, D. Natale, K. Ross, C. Vinayaka, Q. Wang, Y. Wang, L. Yeh, J. Zhang, and U. Consortium. 2017. UniProt: the universal protein knowledgebase. *Nucleic Acids Res* 45:D158-D169.
98. McWilliam, H., W. Li, M. Uludag, S. Squizzato, Y. Park, N. Buso, A. Cowley, and R. Lopez. 2013. Analysis tool web services from the EMBL-EBI. *Nucleic Acids Res* 41:W597-W600.
99. Sievers, F., and D. Higgins. 2018. Clustal Omega for making accurate alignments of many protein sequences. *Protein Sci* 27:135-145.
100. Sali, A., L. Potterton, F. Yuan, H. Van Vlijmen, and M. Karplus. 1995. Evaluation of comparative protein modeling by Modeler. *Proteins* 23:318-326.
101. Laskowski, R. A., M. W. Macarthur, D. S. Moss, and J. M. Thornton. 1993. Procheck - a program to check the stereochemical quality of protein structures. *J Appl Crystallogr* 26:283-291.
102. Søndergaard, C. R., M. H. Olsson, M. Rostkowski, and J. H. Jensen. 2011. Improved treatment of ligands and coupling effects in empirical calculation and rationalization of pKa values. *J Chem Theory Comput* 7:2284-2295.
103. Olsson, M. H., C. R. Søndergaard, M. Rostkowski, and J. H. Jensen. 2011. PROPKA3: consistent treatment of internal and surface residues in empirical pKa predictions. *J Chem Theory Comput* 7:525-537.
104. Jorgensen, W. L., J. Chandrasekhar, J. D. Madura, R. W. Impey, and M. L. Klein. 1983. Comparison of simple potential functions for simulating liquid water. *J Chem Phys* 79:926-935.

105. Lindorff-Larsen, K., S. Piana, K. Palmo, P. Maragakis, J. L. Klepeis, R. O. Dror, and D. E. Shaw. 2010. Improved side-chain torsion potentials for the Amber ff99SB protein force field. *Proteins* 78:1950-1958.
106. Bussi, G., D. Donadio, and M. Parrinello. 2007. Canonical sampling through velocity rescaling. *J Chem Phys* 126:014101.
107. Parrinello, M., and A. Rahman. 1981. Polymorphic transitions in single crystals: A new molecular dynamics method. *J Appl Phys* 52:7182-7190.
108. Nosé, S., and M. L. Klein. 1983. Constant pressure molecular dynamics for molecular systems. Mo*l Phys* 50:1055-1076.
109. Essmann, U., L. Perera, and M. L. Berkowitz. 1995. A smooth particle mesh Ewald method. *J Chem Phys* 103:8577-8593.
110. Allen, M. P., and D. J. Tildesley. 1987. Computer simulation of liquids. Clarendon Press, Oxford, UK.
111. Abraham, M. J., T. Murtola, R. Schulz, S. Pall, J. C. Smith, B. Hess, and E. Lindahl. 2015. GROMACS: high performance molecular simulations through multi-level parallelism from laptops to supercomputers. *SoftwareX* 2:19-25.
112. Delano, W. L. 2003. The Pymol molecular graphics system. version 0.98. Delano Scientific LLC, San Carlos, CA, USA.
113. DeLano, W. L. 2009. PyMOL molecular viewer: updates and refinements. *Abstracts of Papers of the American Chemical Society* 238.
114. Ng, H. W., C. A. Laughton, and S. W. Doughty. 2013. Molecular dynamics simulations of the adenosine A2a receptor: structural stability, sampling, and convergence. *J Chem Inf Model* 53:1168-1178.
115. Kumari, R., R. Kumar, A. Lynn, and O. S. D. D. Consortium. 2014. g_mmpbsa-a GROMACS tool for high-throughput MM-PBSA calculations. *J Chem Inf Model* 54:1951-1962.
116. Baker, N. A., D. Sept, S. Joseph, M. J. Holst, and J. A. McCammon. 2001. Electrostatics of nanosystems: application to microtubules and the ribosome. *Proc Natl Acad Sci U S A* 98:10037-10041.
117. Wood, C. W., A. A. Ibarra, G. J. Bartlett, A. J. Wilson, D. N. Woolfson, and R. B. Sessions. 2020. BAlaS: fast, interactive and accessible computational alanine-scanning using BudeAlaScan. *Bioinformatics* 36:2917-2919.
118. Wood, C. W., J. W. Heal, A. R. Thomson, G. J. Bartlett, A. Ibarra, R. L. Brady, R. B. Sessions, and D. N. Woolfson. 2017. ISAMBARD: an open-source computational environment for biomolecular analysis, modelling and design. *Bioinformatics* 33:3043-3050.
119. McIntosh-Smith, S., J. Price, R. B. Sessions, and A. A. Ibarra. 2015. High performance in silico virtual drug screening on many-core processors. Int J High Perform Comput Appl 29:119-134.
120. Lentz, T. L., T. G. Burrage, A. L. Smith, J. Crick, and G. H. Tignor. 1982. Is the acetylcholine receptor a rabies virus receptor? *Science* 215:182-184.
121. Hueffer, K., S. Khatri, S. Rideout, M. B. Harris, R. L. Papke, C. Stokes, and M. K. Schulte. 2017. Rabies virus modifies host behaviour through a snake-toxin like region of its glycoprotein that inhibits neurotransmitter receptors in the CNS. *Sci Rep* 7:12818.
122. Donnelly-Roberts, D. L., and T. L. Lentz. 1989. Synthetic peptides of neurotoxins and rabies virus glycoprotein behave as antagonists in a functional assay for the acetylcholine receptor. *Pept Res* 2:221-226.
123. Lan, J., J. Ge, J. Yu, S. Shan, H. Zhou, S. Fan, Q. Zhang, X. Shi, Q. Wang, L. Zhang, and X. Wang. 2020. Structure of the SARS-CoV-2 spike receptor-binding domain bound to the ACE2 receptor. *Nature* 581:215-220.

Figure Legends

Figure 1. Overview of the three-dimensional structures of the SARS-CoV-2 spike protein and the αβγδ nAChR from *Tetronarce californica*. (**A)** The model for the complete, fully glycosylated, SARS-CoV-2 spike represents the closed state of the protein, after furin cleavage (55). The spike protein is a homotrimer (42): each monomer is shown in different colours, namely green, cyan and orange, with glycans depicted in pink. Each monomer is formed by three domains: head, stalk and cytoplasmic tail (CT) (42). The Y674-R685 region is shown in red. (**B)** The cryoEM structure of the muscle-type receptor from *Tetronarce californica* (PDB code: 6UWZ) (38). This receptor is a heteropentamer formed of two α (green), one β (blue), one δ (yellow), and one γ (orange) subunits. Each monomer is formed by four domains (28-30): extracellular (ECD), transmembrane (TMD), intracellular (ICD) and C-terminal domain (CTD). The agonist binding site is located in the ECDs at the interface between two neighbouring subunits.

Figure 2. Predicted binding modes of the SARS-CoV-2 S-peptide to different nAChRs. (A) Complexes formed by the S-peptide and three different nAChRs, namely the human α4β2, human α7 and the muscle-like αβγδ receptor from *Tetronarce californica.* The S-peptide (region Y674-R685) is highlighted in magenta, and the principal and complementary subunits of the receptors are coloured in green and cyan, respectively. These models show the conformation of the S-peptide bound to the first pocket at the beginning of the simulations. In the human α4β2 receptor, the binding pocket is formed by one α4 and one β2 subunit, whereas in the human α7 nAChR, the pocket is formed by two α7 subunits. In the αβγδ receptor, the two binding pockets are non-equivalent: one is formed by an α and a δ and the second by an α and a γ subunits. (**B)** Closeup view of the peptide-receptor interaction region. Residues involved in binding of the S-peptide are shown with sticks. Note that the sidechain of R682 in the S-peptide is located inside the aromatic box establishing cation-π interactions with some of the highly conserved aromatic residues lining the pocket. Note also that all residue numbers used in this work, unless stated otherwise, refer to the human α7 (UniProt code P36544), human α4 (UniProt code P43681), human β2 (UniProt code P17787), *Tetronarce californica* α (UniProt code P02710), *Tetronarce californica* δ (UniProt code P02718), *Tetronarce californica* γ (UniProt code P02714) and SARS-CoV-2 spike protein (Uniprot code P0DTC2) sequences.

Figure 3. Representative conformation of the α7 complex, in which direct interaction between TrpB and R682 is observed. **(A)** Overall view of the S-peptide:α7 complex. (**B)** Closeup view of the R682 interaction region within the aromatic box. The principal and complementary subunits of the α7 receptor are coloured in green and cyan, respectively. The S-peptide is highlighted in magenta. Interactions between the guanidinium group of R682 and the aromatic rings of TrpB (α7W171),

TyrC1 (α7Y210) and TyrC2 (α7Y217) are shown with dashed lines. See also Figures S13-S16 for more details about the behaviour of the S-peptide when bound to α7 nAChR.

Figure 4. Accessible surface area (ASA) of Y674-R685 region in the context of the fully glycosylated full-length SARS-CoV-2 spike. (**A**) A snapshot taken from the simulations by Casalino *et al.* (55) of the glycosylated full-length SARS-CoV-2 spike in the closed state showing Y674-R685 loop protruding into the solvent. The protein is depicted with a grey surface, whereas 674-685 loop is shown as a cyan ribbon. The glycans are illustrated with blue sticks. (**B-C**) The ASA of the of residues 674-685 (corresponding to the S-peptide), and the area shielded by glycans, at multiple probe radii from 1.4 Å (water molecule) to 15 Å are calculated using the available MD trajectories of the full-length models of the glycosylated SARS-CoV-2 spike protein in the closed (**B**) and open states (**C**) from Casalino *et al.* (55). The area of 674-685 shielded by the glycans is presented in blue, whereas the grey line represents the accessible area of 674-685 in the absence of glycans. Highlighted in cyan is the area of 674-685 that remains accessible in the presence of glycans. The calculated values have been averaged across the three chains and across the different replicas performed for each system by Casalino *et al.* (55). Error bars correspond to +/- standard deviation.